Slip on Superhydrophobic Surfaces

Jonathan P. Rothstein

Department of Mechanical and Industrial Engineering, University of Massachusetts, Amherst, Massachusetts 01003; email: rothstein@ecs.umass.edu

Annu. Rev. Fluid Mech. 2010. 42:89–109

First published online as a Review in Advance on August 17, 2009

The *Annual Review of Fluid Mechanics* is online at fluid.annualreviews.org

This article's doi:
10.1146/annurev-fluid-121108-145558

0066-4189/10/0115-0089$20.00

Key Words

drag reduction, lotus effect, ultrahydrophobic

Abstract

This review discusses the use of the combination of surface roughness and hydrophobicity for engineering large slip at the fluid-solid interface. These superhydrophobic surfaces were initially inspired by the unique water-repellent properties of the lotus leaf and can be employed to produce drag reduction in both laminar and turbulent flows, enhance mixing in laminar flows, and amplify diffusion-osmotic flows. We review the current state of experiments, simulations, and theory of flow past superhydrophobic surfaces. In addition, the designs and limitations of these surfaces are discussed, with an eye toward implementing these surfaces in a wide range of applications.

INTRODUCTION

Friction in fluids is manifest by the phenomenon of drag—the force required to move an object through a fluid or move a fluid through a device. A number of recent reviews discuss the validity of the no-slip boundary condition in fluid dynamics (Bouzigues et al. 2008, Lauga et al. 2007, Vinogradova 1999, Voronov et al. 2008). This review focuses on a special class of materials called superhydrophobic surfaces that have been used recently to engineer large slip. These surfaces enhance the mobility of drops by reducing their contact-angle hysteresis and reduce drag in both laminar and turbulent flows by supporting a shear-free air-water interface over which water slips. Drag reduction in turbulent flows can be achieved through a number of different mechanisms. However, in pressure-driven laminar flows, the use of superhydrophobic surfaces represents one of the first technologies capable of reducing drag in devices that are larger than the molecular scale. The development of these surfaces (given their ability to produce significant drag reduction over a broad range of Reynolds numbers, both laminar and turbulent) could profoundly affect a variety of important existing technologies, from microfluidic devices to marine vessels. Below we describe the recent literature and advances in the use of superhydrophobic surfaces over a broad range of fluid applications.

VALIDITY OF THE NO-SLIP BOUNDARY CONDITION

The no-slip condition is accepted almost universally as the proper boundary condition to impose at a solid-liquid interface. The validity of the no-slip boundary condition, however, was debated quite extensively throughout the nineteenth and early twentieth century by some of the greatest scientific minds of the time (Goldstein 1965). In the end, its implementation arose from a wealth of experimental validation. It should be emphasized that the no-slip boundary condition is no more than a convenient approximation that has been found to hold under most normal flow conditions (Batchelor 1985).

The concept of a slip boundary condition was first proposed by Navier (1823) and is shown schematically in **Figure 1**. In Navier's model, the magnitude of the slip velocity, u_0, is proportional to the magnitude of the shear rate experienced by the fluid at the wall:

$$u_0 = b \left| \frac{\partial u}{\partial y} \right|, \tag{1}$$

where b is the slip length. Maxwell was the first to quantify the slip length of gas flowing past a solid surface. His calculations predicted a slip length that is on the order of the mean free path of

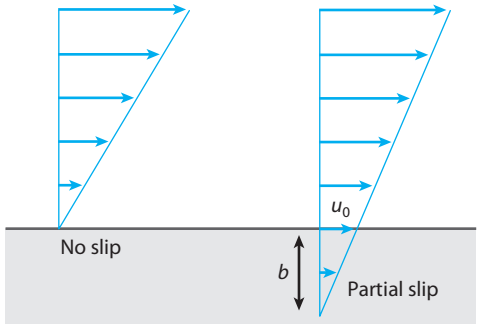

Figure 1

Schematic diagram of slip at a fluid-solid interface.

the fluid, λ (Maxwell 1879). This theory was later made quite rigorous by Tolstoi (1952) and then Blake (1990). Thus, for nearly all macroscopic flows of simple fluids, the slip length is so small, $b = \mathrm{O}(1\,\mathrm{nm})$, that it can be neglected, and the no-slip boundary condition can be used without loss of accuracy.

One well-known exception to the use of the no-slip boundary condition is any flow in which the mean free path of the fluid approaches the characteristic length scale, L_c, of the device. For flows of rarified gases or flows within microfluidic or nanofluidic devices in which the Knudsen number is greater than $Kn = \lambda/L_c > 0.1$, slip has been shown to be important (Karniadakis et al. 2005). Additionally, in flows with an advancing free surface, there is a boundary-condition discontinuity at the intersection of the moving free surface and the solid boundary. Examples of such situations include the spreading of a drop on a solid substrate and the extrusion of a polymer melt. In these flows, the use of the no-slip boundary condition would produce a nonphysical result (Denn 2001, Dussan 1979), and a finite slip length is often employed, even in these macroscopic flows, to eliminate the resulting velocity singularity (Hocking 1976). Molecular dynamics simulations have shown this approach to be quite appropriate (Freund 2003).

As microfluidic devices have become more widely used, it is has become extremely desirable to develop fluid-surface parings that can achieve slip lengths on the order of micrometers rather than nanometers. Let us take, for example, the pressure-driven flow between two infinite parallel plates separated by a distance H. If one of these plates can support slip, the volume flow rate per unit depth is given by

$$q = \frac{H^3}{4\mu}\left(-\frac{dp}{dx}\right)\left[\frac{1}{3} + \frac{b}{b+H}\right]. \qquad (2)$$

For a given pressure gradient, dp/dx, and fluid viscosity, μ, the volume flow rate can be significantly enhanced if and only if the slip length is on the order of the channel height. A number of recent studies have focused on quantifying the magnitude of the slip length and its dependence on parameters such as wettability and surface roughness (Lauga et al. 2007, Vinogradova 1999).

The wettability of a surface is defined by the spreading coefficient, $S = \gamma_{SV} - \gamma_{LV} - \gamma_{LS}$, where γ_{SV}, γ_{LV}, and γ_{LS} are the solid-vapor, liquid-vapor, and liquid-solid interfacial tensions, respectively (Israelachvili 1992). For spreading coefficients greater than zero, $S > 0$, the solid is fully wetted by the liquid, whereas for $S < 0$, the solid is only partially wet by the liquid, which forms a spherical end cap with an equilibrium contact angle defined by Young's (1805) law as $\theta = \cos^{-1}[(\gamma_{SV} - \gamma_{LS})/\gamma_{LV}]$. For surfaces with contact angles less than $\theta < 90°$, the surface is considered hydrophilic, whereas for those with $\theta \geq 90°$, the surface is hydrophobic. However, as discussed in more detail below, reporting only the equilibrium contact angle for a surface is insufficient. Owing to the presence of surface roughness or chemical heterogeneity, a liquid droplet can actually exist over a range of contact angles between the receding contact angle, θ_R, and the advancing contact angle, θ_A (de Gennes et al. 2004). This nonuniqueness of the equilibrium contact angle is known as the contact-angle hysteresis, $\theta_R - \theta_A$ (Gao & McCarthy 2006a).

The first results showing that surface hydrophobicity can produce slip lengths much larger than the mean free path were the molecular dynamic simulations of Thompson & Troian (1997) and Barrat & Bocquet (1999). Thompson & Troian (1997) showed that at large shear rates, nonlinear effects become important and the calculated slip length diverged as the applied shear rate approached a critical shear rate. This critical shear rate decreased with decreasing surface energy corrugation at the wall, which, in a macroscopic sense, corresponds to an increasing contact angle between the liquid and the solid. Later, Barrat & Bocquet (1999) showed that, even at shear rates at which the slip length has been found to be constant and independent of the shear rate (for fluid-surface contact angles of $\theta = 140°$ or more), slip lengths greater than 40 molecular diameters,

$b > 40\sigma$, could be achieved at modest static pressures. This result contrasts with hydrophilic and even moderately hydrophobic surfaces, $\theta < 100°$, for which, as expected, slip lengths of only a couple of molecular diameters were predicted. The enhancement of the slip length resulted from a liquid depletion layer near the wall. Within this layer, both the density and the fluid viscosity are reduced, resulting in large velocity gradients near the hydrophobic wall and an apparent slip length that is large enough that it should be experimentally verifiable. For a number of lengthy reviews of the more recent simulation results, the reader is referred to Voronov et al. 2008 and Lauga et al. 2007.

Although the technologies to probe the fluid dynamics at the nanometer length scales required to measure slip have been available for some time, the experimental challenges of these measurements only recently have been overcome sufficiently such that consistent measurements over a wide variety of techniques can be made. A number of studies have calculated slip lengths indirectly from pressure-drop (Choi et al. 2003, Schnell 1956) or friction-factor measurements (Baudry et al. 2001; Cottin-Bizonne et al. 2005; Zhu & Granick 2001, 2002) of simple fluids flowing past nonwetting smooth surfaces. Cottin-Bizzone and coworkers (2005) used a modified surface force apparatus to investigate the hydrodynamics of water and dodecane confined between a hydrophilic Pyrex sphere and either a hydrophilic Pyrex plane or a hydrophobic Pyrex plane coated with octadecyltrichlorosilane (OTS). Using a periodic squeezing flow with nanometer-size oscillations, they measured the hydrodynamic forces and calculated the resulting slip length. In their experiments, slip lengths of approximately $b \approx 20$ nm were found for the hydrophobic surface, whereas the hydrophilic surface was found to have no measurable slip length. The surfaces had a root-mean-square (RMS) roughness of approximately 1 nm. Similar measurements with other surfaces showed that the maximum slip length corresponded to the surfaces with the smallest RMS roughness (Zhu & Granick 2002). The rougher surfaces regained some degree of slip at large shear rates as it is thought that they may induce nanobubble cavitation (Cottin-Bizonne et al. 2003), resulting in an early onset of the nonlinear effects predicted by Thompson & Troian (1997).

Only a few direct measurements of the slip velocity itself have been made at or near the wall in flows over smooth hydrophobic surfaces because of the small slip lengths and slip velocities (Jin et al. 2004, Joly et al. 2006, Joseph & Tabeling 2005, Pit et al. 1999). Using micro-particle image velocimetry (μ-PIV) measurements, Joseph & Tabeling (2005) found a slip length for the flow of water through a microchannel coated with a monolayer of hydrophobic octadecyltrichlorosilane to be approximately $b \approx 30$ nm. However, as with many of the earlier μ-PIV experiments that measured much larger slip lengths (Tretheway & Meinhart 2002), measured values of the slip length were well within the error of the velocity measurements. There were two major sources of uncertainty in these μ-PIV measurements: (*a*) the certainty to which the investigators could locate the wall and (*b*) the uncertainty of the location of the tracer particles, which tend to migrate away from the wall and are typically much larger than the slip lengths they are being used to measure. As the state of the art of μ-PIV has improved, measurement error has been reduced significantly, as has the typical value of the slip lengths measured.

Other techniques besides μ-PIV have also been utilized to measure the slip length in flows past smooth hydrophobic surfaces. Pit et al. (1999) used total internal reflection fluorescence microscopy (TIRF) to measure the fluorescence recovery after photobleaching and determine the slip velocity of hexadecane flowing past a lyophobically modified, smooth sapphire surface. The use of TIRF allowed Pit et al. (1999) to probe the fluid velocity in close proximity (<100 nm) to the solid surface with a precise knowledge of the particle position. More recently, Jin et al. (2004) combined TIRF of submicrometer particles with particle tracking velocimetry (PTV) to measure the velocity of water near a glass surface coated with a self-assembled monolayer of OTS. They

measured slip lengths less than $b < 10$ nm. Their measurements brought to light a number of features regarding the motion of the passive tracer particles in close proximity to a wall that could have negatively affected previous μ-PIV and PTV measurements. These features included the non-Gaussian Brownian motion of the particles near the wall and the hindered diffusion of the particles owing to near-wall lubrication effects. Joly et al. (2006) utilized the latter phenomena to make accurate measurements of slip length. They used PTV of particles under only Brownian motion to investigate the effect of confinement (proximity of particle to the wall) on the diffusion coefficient of the particles. For a hydrophilic surface, the reduction in the diffusion coefficient with proximity to the wall was well matched by the predictions of numerical simulations for particle motion above a no-slip surface. However, for a hydrophobic OTS-coated silica plane, the diffusion coefficient data matched simulations for a surface having a slip length of $b = 18$ nm. Joly et al. (2006) also investigated the role of roughness on the slip length and found that the addition of even a modest RMS roughness of 3 nm caused the OTS-coated surface to revert back to no slip. Their measurements thus showed that, in the absence of trapped air within the contours of the rough surface (Cottin-Bizonne et al. 2004, Ou et al. 2004), slip larger than a few tens of nanometers cannot be achieved. Achieving slip lengths on the order of micrometers rather than nanometers necessitates the use of superhydrophobic surfaces.

SUPERHYDROPHOBIC SURFACES

Superhydrophobic surfaces were originally inspired by the unique water-repellent properties of the lotus leaf (Barthlott & Neinhuis 1997) and the leaves of a number of other plants (Bhushan & Jung 2006). It is the combination of a very large contact angle and a low contact-angle hysteresis that defines a surface as superhydrophobic. The lack of significant contact-angle hysteresis makes a water drop on a superhydrophobic surface unstable to even the smallest perturbation and allows it to move easily across these surfaces (Bico et al. 1999, Chen et al. 1999, Kim & Kim 2002, Sakai et al. 2006, Shastry et al. 2006). This can be seen explicitly if one calculates the critical line force required to start a drop moving over a solid surface (Wolfram & Faust 1978):

$$F = \pi r \gamma_{LV} (\cos \theta_R - \cos \theta_A), \tag{3}$$

where r is the radius of the contact line. Any significant contact-angle hysteresis can result in the drop becoming pinned to a surface even as that surface is tilted through vertical (Quéré et al. 1998). For superhydrophobic surfaces, drops tend to roll rather than slide because the large contact angle moves the center of mass well above the surface (Mahadevan & Pomeau 1999). Rolling water drops tend to collect and remove dirt as they go, resulting in the remarkable self-cleaning ability of the lotus leaf and other superhydrophobic surfaces. In addition to plants, there are a large number of animals and insects that have evolved unique ways to utilize superhydrophobicity (Bush et al. 2008). Water striders, for example, have legs with thousands of tiny hydrophobic hairs or microsetae that allow them to stand and move quickly on water (Gao & Jiang 2004).

Synthetic superhydrophobic surfaces have recently been developed that are capable of obtaining contact angles that approach $\theta \approx 180°$ with little to no measurable hysteresis (Gao & McCarthy 2006c, Quéré 2008, Reyssat et al. 2008). Importantly, the difference between a hydrophobic surface and a superhydrophobic surface lies not in the surface chemistry, but in the micro- or nanoscale surface roughness. Lotus leaves, for example, have micrometer-sized protrusions covered in hydrophobic wax crystalloids (Barthlott & Neinhuis 1997). For a rough surface like that of a lotus leaf, water will either fully or partially wet the surface depending on the hydrophobicity of the surface, the static pressure in the water, and the precise geometry of the surface features.

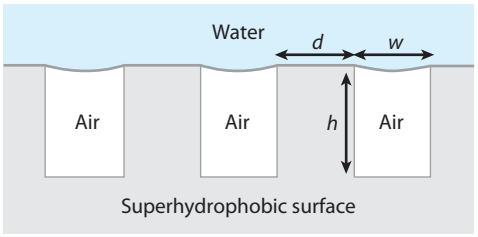

Figure 2

Schematic diagram of a superhydrophobic surface in the Cassie state.

In the Wenzel (1936) state, water penetrates the corrugations on the surface. In this state, the hydrophobicity is enhanced by the roughness of the surface:

$$\cos\theta_W = r\cos\theta, \tag{4}$$

where θ_W is the equilibrium contact angle in the Wenzel state, and r is a roughness parameter that is the ratio of the actual wetted area to the projected area of the surface. For a periodic array of square posts with the dimensions shown in **Figure 2**, the roughness parameter is given by $r = 1 + 4\phi_s h/d$, where $\phi_s = d^2/(d+w)^2$ is the fraction of surface covered by posts. In the Wenzel state, the equilibrium contact angle can be increased systematically for a hydrophobic surface by increasing either the aspect ratio or density of the posts. The contact-angle hysteresis in the Wenzel state is typically quite large because the contact line is pinned quite effectively along the sides and corners of the posts (Lafuma & Quéré 2003).

In the Cassie state (Cassie & Baxter 1944), the hydrophobicity of the microscale surface roughness prevents the water from moving into the space between the peaks of the surface roughness, resulting in an air-water interface supported by the posts as seen schematically in **Figure 2**. The equilibrium contact angle in the Cassie state increases in proportion to the amount of air-water interface present, $(1 - \phi_S)$, such that

$$\cos\theta_C = -1 + \phi_S(1 + \cos\theta). \tag{5}$$

In addition to an increase in the equilibrium contact angle, the presence of the air-water interface also minimizes the contact-angle hysteresis as the contact line is only pinned along the solid fraction of the surface. Oner & McCarthy (2000) showed that the contact-angle hysteresis is also a function of post shape, size, and density. It is thus the Cassie state that is truly superhydrophobic. To simultaneously maximize the contact angle and minimize the hysteresis, one needs to reduce the density of posts. There is, however, a practical limit on the post density. For a droplet in the Cassie state, there is a maximum static pressure that can be supported before the air-water interface deflects enough to reach the advancing contact angle and is driven into the space between the surface roughness. At this point the system reverts to the Wenzel state. Using Young's law and assuming an interface with a single radius of curvature such as that which exists between two parallel ridges as seen in **Figure 2**, we find that

$$\Delta p_{max} = p_{water} - p_{air} = -\frac{2\gamma\cos\theta_A}{w}. \tag{6}$$

Thus, the maximum static pressure that can be supported in the Cassie state decreases with increasing feature spacing. A similar conclusion can be reached using an energy argument. For a transition to occur from the Cassie to the Wenzel state, the gain in interfacial energy due to the increase in wetted area must be less than the work gained by displacing the interface into the surface texture, $\Delta E < W$. For an array of square posts, the change in interfacial energy is given

by $\Delta E = (\gamma_{LS} - \gamma_{SV} - \gamma_{LV})[(d + w)^2 - d^2] + 4dh(\gamma_{LS} - \gamma_{SV})$ while the work gained by displacing the interface is given by $W = (p_{water} - p_{air})[(d + w)^2 - d^2]h$. The maximum sustainable pressure difference thus becomes

$$\Delta p_{max} = p_{water} - p_{air} = \frac{(\gamma_{LS} - \gamma_{SV} - \gamma_{LV})}{h} - \frac{4d\gamma_{LV}\cos\theta}{[(d + w)^2 - d^2]}. \quad (7)$$

Beyond this pressure difference, the surface will spontaneously transition from the Cassie to the Wenzel state. Note that in the limit of tall posts spaced far apart, Equations 6 and 7 are equivalent.

For a hydrophobic surface, the dry surface has a lower surface energy than the wetted surface, so it is natural to assume that a drop would exist in the Cassie state as long as the criteria in Equations 6 and 7 were satisfied. However, Bico et al. (2002) showed that for contact angles between $\pi/2 < \theta < \theta_{crit}$, where $\cos\theta_{crit} = (\phi_s - 1)/(r - \phi_s)$, the Cassie state is metastable. In this range of contact angles, the existence of an air-water interface depends on how the surface is prepared; deposition of large drops on top of the features will result in the Cassie state, whereas condensation of water vapor from the air will result in the Wenzel state (Wier & McCarthy 2006).

The dynamics of water drops on superhydrophobic surfaces such as those shown in **Figure 3** have been considered in the recent literature. Kim & Kim (2002) experimentally studied the flow resistance of water drops sliding down inclined surfaces in both open and confined channel geometries. They fabricated the channels out of superhydrophobic silicon surfaces with arrangements of both micropost and nanopost patterns. Measurements of the minimum inclination angle required to initiate flow demonstrated drag reductions of 60% for the micropost patterns and 99% for the nanopost patterns (Kim & Kim 2002). The observed drag reductions of Kim & Kim and others (Sakai et al. 2006, Shastry et al. 2006) correlated directly with the contact-angle hysteresis of the surfaces as demonstrated by Equation 3. Richard & Quéré (2000) showed that water drops will bounce with a very high coefficient of restitution on superhydrophobic surfaces. More recently, Reyssat et al. (2006) and Bartolo et al. (2006) demonstrated that above a critical impact velocity, the impacting drop cannot be supported completely in the Cassie state as the supported air-water interface is driven into the Wenzel state by the force of impact. As a result, a partial pinning of the droplet is observed, followed by peripheral fragmentation of the spreading drop at even larger impact velocities. Additionally, a number of recent papers have demonstrated that gradients in contact angle on a superhydrophobic surface imposed by varying the post or ridge

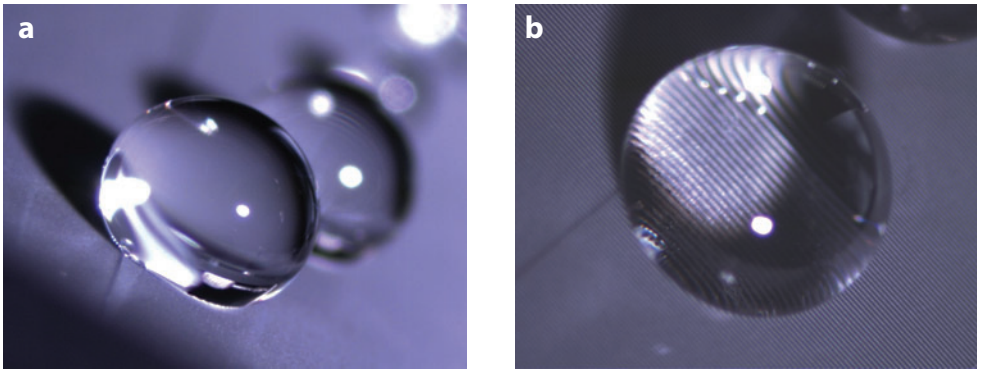

Figure 3

Water drops on a superhydrophobic surface consisting of 15 μm wide ridges spaced 45 μm apart seen from (*a*) the side and (*b*) the top. Note that the ridges and the air-water interface supported between them are visible through the drop in the top view (*b*).

spacing or size could induce drop motion in the direction of decreasing advancing contact angle (Fang et al. 2008, Shastry et al. 2006, Yang et al. 2006).

SLIP ON SUPERHYDROPHOBIC SURFACES: LAMINAR FLOWS

Experimental Results

Under pressure-driven laminar flow conditions, drag reduction can be difficult to achieve. Ou and colleagues (2004; Ou & Rothstein 2005) were among the first to demonstrate experimentally that superhydrophobic surfaces could reduce drag in laminar flows. In flows over superhydrophobic surfaces, the boundary condition experienced by the fluid in contact with the solid is no slip; however, the air-water interfaces supported between the micro- or nanofeatures are essentially shear-free. Using a series of lithographically etched and silanized silicon surfaces with precisely controlled microsurface topology consisting of regular arrays of microposts and microridges, Ou and colleagues systematically investigated the effect of topological changes on the flow through a series of microchannels of varying height. As shown in **Figure 4**, they achieved in some cases drag reductions greater than $D_R = (\Delta p_{no-slip} - \Delta p_{SH})/\Delta p_{no-slip} > 40\%$, corresponding to slip lengths greater than $b > 25$ μm. For the flows through these microchannels, the Knudsen numbers were all less than $Kn < 10^{-4}$, and thus the large slip lengths measured are clearly not due to noncontinuum effects. Ou and colleagues showed that drag reduction and slip length increased with increasing shear-free area, increasing spacing between microfeatures and decreasing channel height. The trends for microridges and microposts were similar and well matched by the predictions of computation fluid dynamics (CFD) simulations. However, when the two sets of data are

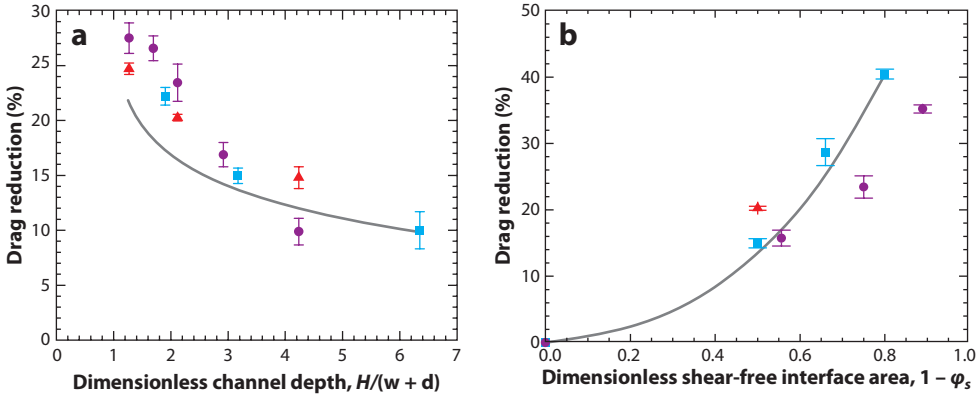

Figure 4

The average drag reduction as a function of (*a*) dimensionless channel depth and (*b*) percentage of shear-free interface. The data in panel *a* include superhydrophobic surfaces with a regular array of 30 μm wide microridges spaced 30 μm apart (*red triangles*), 20 μm wide microridges spaced 20 μm apart (*blue squares*), and 30 μm square microposts spaced 30 μm apart (*purple circles*) for a variable height microchannel. In panel *b*, the features are the same size, but the spacing between them is varied. Additionally, the microchannel is 2.54 mm wide, $H = 127$ mm high, and 50 mm long. Superimposed on both data sets are the predictions of computation fluid dynamics simulations for the 20 μm wide microridges spaced 20 μm apart case (*gray line*). Figure adapted with permission from Ou and Rothstein, 2005, Direct velocity measurements of the flow past drag-reducing ultrahydrophobic surfaces, *Phys. Fluids*, 17:103606, Copyright 2005, American Institute of Physics and reprinted with permission from Ou, Perot, and Rothstein, 2004, Laminar drag reduction in microchannels using ultrahydrophobic surfaces, *Phys. Fluids*, 16:4635–60, Copyright 2004, American Institute of Physics.

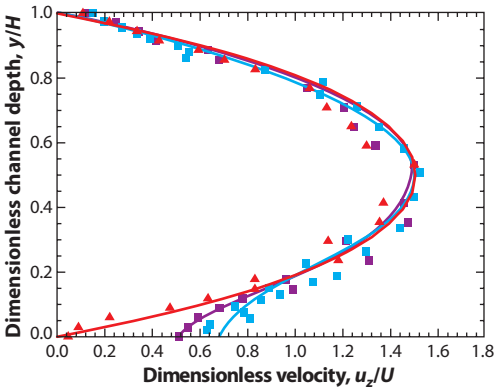

Figure 5

Velocity profiles measured through micro-particle image velocimetry (μ-PIV) for the flow through an $H = 85$ μm tall microchannel past a series of superhydrophobic surfaces containing $w = 30$ μm wide microridges spaced $d = 30$ μm (*red and purple symbols*) and $d = 60$ μm (*blue symbols*) apart. The data include the velocity profile for a vertical slice taken above the center of the microridge (*red triangles*), above the center of the 30 μm shear-free interface (*purple squares*), above the center of the 60 μm shear-free interface (*blue squares*), and the corresponding predictions of the computational fluid dynamics simulations (*lines*). Figure reprinted with permission from Ou & Rothstein 2005, Direct velocity measurements of the flow past drag-reducing ultrahydrophobic surfaces, *Phys. Fluids*, 17:103606, Copyright 2005, American Institute of Physics.

compared as a function of the fraction of shear-free area, the microridges consistently outperform the microposts.

Ou et al. (2004) demonstrated the existence and subsequent deflection of the air-water interface under flow through laser confocal surface metrology measurements of the interface. In their later work, Ou & Rothstein (2005) used μ-PIV measurements to systematically and precisely probe the detailed flow kinematics throughout the microchannel at length scales well below that of the microridges on the superhydrophobic surface. An example of the resulting velocity profile is shown in **Figure 5**. Whereas the flow was observed to come to rest along the microridges, along the air-water interface, slip velocities greater than 60% of the average velocity were measured. The velocity profile across the air-water interface was parabolic with a maximum velocity at the center of the interface that increased with increased spacing between the microridges. These measurements demonstrated a direct correlation between the increase in the pressure-drop reduction and the increase in the slip velocity along the shear-free air-water interface.

A number of more recent experiments have extended these results to a variety of superhydrophobic surface designs and flow geometries (Choi & Kim 2006, Choi et al. 2006, Joseph et al. 2006, Truesdell et al. 2006). Some of these studies have moved toward superhydrophobic surfaces with nanometer-sized features. Choi et al. (2006) studied a superhydrophobic surface created using a Teflon-coated nanograting with a 60 nm wide ridge spaced 180 nm apart. They used a specially designed flow meter to measure differences in the throughput of a microfluidic device between smooth and superhydrophobic surfaces and infer slip lengths. They found slip lengths of roughly $b \approx 140$ nm for flow parallel to the ridge direction and roughly half that length for flow transverse to the ridge direction. Choi & Kim (2006) created needle-like structures on a silicon wafer using the black silicon method. The resulting nanoturf consisted of 1 to 2 nm tall nanoposts spaced 500 nm to 1 μm apart, which were coated with Teflon to make the surface hydrophobic. They measured drag reduction using a cone-and-plate rheometer. Slip lengths of approximately $b \approx 20$ μm and $b \approx 50$ μm were determined for water and for glycerin, respectively. We note that there is

some question about the accuracy of slip measurements using cone-and-plate rheometers as the uncertainty in the slip length can be of the same order as the reported values for water (Bocquet et al. 2006).

Joseph et al. (2006) created a similar nanoturf surface using a surface carpeted with random arrays of bundled carbon nanotubes. In their experiments, they measured the slip length using μ-PIV. The average separation of the carbon nanotube bundles was measured through scanning electron microscopy, and the slip length was measured as a function of this separation for both hydrophobic and hydrophilic surfaces. For the hydrophobic surface, the Cassie state was maintained, and Joseph et al. (2006) measured slip lengths in the micrometer range that increased with the increased separation between posts. When the nanoposts were wetted in the Wenzel state, a no-slip boundary condition was recovered.

A number of other groups have also been engineering superhydrophobic surfaces to maximize their drag-reducing ability. Lee et al. (2008) used deep reactive ion etching on silicon to produce superhydrophobic surfaces with microposts and microridges that approach a solid fraction of $\phi_s \rightarrow 0$. A shear rheometer was again used; however, the slip measurements were so large that the experimental error could not compromise the data in this case. Lee et al. (2008) measured slip lengths that approached $b \approx 200$ μm. We note that these experiments were performed at the very limit for which a stable interface could be maintained in the Cassie state. Additionally, the experiments showed that at very low solid fractions, arrays of microposts outperform microridges for the same fraction of shear-free area. This contrasts with the results observed at a higher solid fraction but is in good agreement with the predictions of theory and CFD simulations.

Theoretical and Computational Results

Philip (1972a,b) was the first to theoretically study the flow past a series of idealized superhydrophobic surfaces, although his motivation was to understand the flow through porous media and not necessarily drag reduction. Philip (1972a,b), and more recently Lauga & Stone (2003) and Cottin-Bizonne et al. (2004), analytically solved the Stokes flow problem of flow past surfaces or through channels with mixed boundary conditions. With a few notable exceptions, analytical theory and, for that matter, numerical simulations involving flow past superhydrophobic surfaces typically assume that the air-water interface is flat and shear-free and that the viscosity (and therefore flow resistance) of the air trapped within the surface features is negligible. The analytical solutions covered a range of different geometries, including a circular tube, two parallel plates, and a single infinite plate. Additionally, the superhydrophobic surfaces studied contained either a single or a periodic array of shear-free bands running parallel or transverse to the flow direction. The solutions predict that for a given flow geometry, the drag reduction is a function of both the fraction of shear-free area and the dimensionless channel depth or radius, $D_R = f(\phi_s, H/[w+d])$, whereas the slip length is independent of channel height or radius but is a function of the dimensional period of the roughness, $b = f(\phi_s, [w+d])$.

Recently, Ybert et al. (2007) performed a nice scaling analysis for the slip length along superhydrophobic surfaces with generic surface roughness. Following their analysis, if we assume that the air-water interface is shear-free, then the shear stress at the superhydrophobic surface is produced only along the tops of the solid posts or ridges, $\tau = \phi_s \mu \dot{\gamma}$. In the creeping flow regime, the region of the flow influenced by the presence of the top of the post or ridge scales with its size. The shear rate can thus be approximated as $\dot{\gamma} = U/d$, and the shear stress becomes $\tau = \phi_s \mu U/d$, where U is the average flow velocity. Using the definition of slip length in Equation 2, we can alternatively

rewrite the shear stress as $\tau = \mu u_0/b$. Finally, in the limit that the solid fraction is small, $\phi_s \to 0$, the slip velocity approaches the bulk velocity $u_0 \sim U$, and the slip length becomes $b \sim d/\phi_s$. For a superhydrophobic surface of microridges, this analysis shows that the slip velocity should be directly proportional to the period of the microridges, $b \sim d + w$. This result is in agreement with the exact solution of Philip (1972a,b) up to a slowly varying logarithmic dependence on the solid fraction, $b \sim (d + w) \ln(1/\phi_s)$. For the case of microposts, a stronger dependence on solid fraction is predicted by Ybert's theory, $b \sim (d + w)/\phi_s^{1/2}$. The predictions of this scaling argument have been verified recently by experiments with vanishingly small solid fractions (Lee et al. 2008).

A number of different authors have performed CFD simulations to better understand superhydrophobic drag reduction and to extend the analytical solutions beyond their idealized description of the superhydrophobic surface. The first simulations were performed using molecular dynamics with nanometer-sized features (Cottin-Bizonne et al. 2003, 2004), whereas more recent simulations have used finite elements (Maynes et al. 2007, Ou & Rothstein 2005) or lattice Boltzmann simulations (Harting et al. 2006, Hyvaluoma & Harting 2008, Sbragaglia et al. 2006). In general, and as seen in **Figures 4** and **5**, the predictions of the CFD simulations agreed well with both experimental velocity profiles and drag-reduction data.

The continuity and shape of the air-water interface have been shown to be an important factor in drag reduction. Steinberger et al. (2007) used a modified surface force apparatus to investigate the hydrodynamics of a water-glycerol mixture confined between a sphere and a superhydrophobic surface containing a square array of $d = 1.3\,\mu$m holes with a center-to-center spacing of $L = 1.4\,\mu$m. Their measurements showed a slip length of approximately $b \approx 20$ nm for their bubble mattress. This value is an order of magnitude smaller than what has been achieved for the inverted surface (posts) rather than holes with similar dimensions. Their findings demonstrate the importance of designing superhydrophobic surfaces with a contiguous air-water interface in the flow direction such as is present between an array of ridges or posts. It also suggests the reason that, for the same solid fraction, posts are less effective than ridges: The air-water interface between adjacent posts in the flow direction is trapped. The fluid along a trapped air-water interface cannot achieve a large slip velocity because the fluid must, for example, accelerate from rest at the trailing edge of one post and decelerate back to rest at the leading edge of the next post.

Another interesting finding from Steinberger et al. (2007) is that for bubble mattresses studied, a larger slip length was actually achieved for the hydrophilic, fully wetted holes in the Wenzel state, $b \approx 105$ nm, than the hydrophobic Cassie state, $b \approx 20$ nm. The authors performed a series of numerical simulations in which they studied the effect of interface shape on the resulting slip length. They found that the maximum drag reduction was achieved when the air-water interface supported above the holes was flat and dropped off quite significantly for menisci that protruded into the flow or into the holes. Sbragaglia & Prosperetti (2007) found similar results for the flow past microridges supporting deformed interfaces. Steinberger et al. (2007) showed that the immobility of the air-water interface and the resulting blockage of the flow combine to actually enhance drag for bubbles protruding beyond $\theta > 60°$. In a recent study, Hyvaluoma & Harting (2008) used lattice Boltzmann simulations to show that at large capillary numbers, at which the bubbles are deformed by the flow, the slip length can be further reduced by interface protrusion. These results are in agreement with Richardson's (1973) predictions that the proper macroscopic boundary condition for a perfectly shear-free surface will become no slip if the surface is sufficiently rough. These results also cast doubt on whether the presence of nanobubbles can be responsible for some of the anomalously large slip length measurements on smooth hydrophobic surfaces (Lauga et al. 2007).

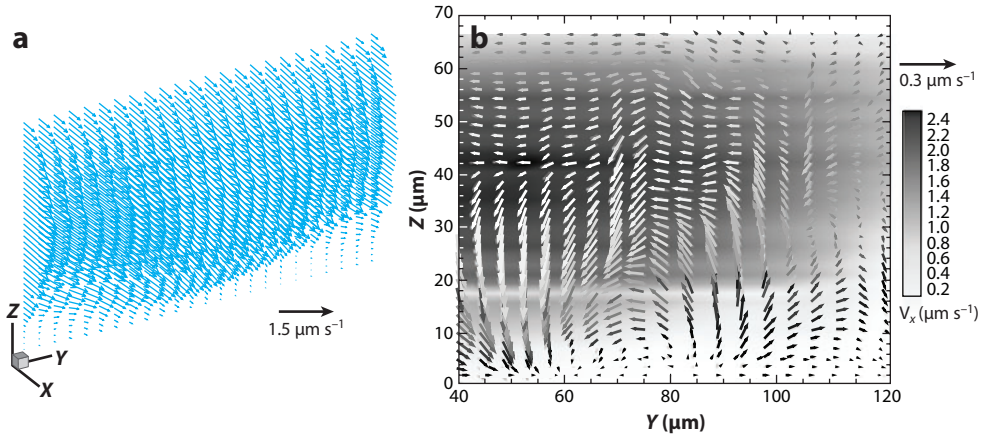

Figure 6

(*a*) A three-component velocity profile at a plane 130 μm from the entrance of a mixing channel 100 μm wide and 65 μm deep with a superhydrophobic surface with 30 μm microridges spaced 30 μm apart at a 45° angle to the flow direction on one wall. The flow rate was 1 ml min^{-1}. (*b*) The *y* and *z* component of the velocity as a vector superimposed over a color contour of the *x* component of the velocity. Figure reprinted with permission from Ou J. 2007. *Laminar flow control using ultrahydrophobic surfaces*. Ph.D. thesis. University of Massachusetts, Amherst, Copyright 2007, University of Massachusetts.

Enhanced Mixing

Superhydrophobic surfaces have recently found application in microfluidic devices in which they can enhance mixing. Under laminar, microscale flow conditions, rapid mixing can be difficult to achieve. In these low–Reynolds number flows, mixing rates are governed by molecular diffusion, and in the absence of enhanced mixing techniques, mixing lengths and residence times can be much longer than most applications allow. By using a superhydrophobic surface consisting of microridges at an oblique angle to the flow direction, Ou et al. (2007) generated a secondary helical flow down the length of the channel and a tertiary flow near the superhydrophobic surface that efficiently reduced the mixing length by more than an order of magnitude compared with that of a smooth microchannel. Using a conservation of mass technique, Ou (2007) made three-dimensional, three-component velocity vector field measurements of the mixing flow. An example of one of these profiles is presented in **Figure 6**. Through the alignment of the microposts at a 45° angle to the flow direction, the fluid was deflected by an angle of approximately 2° from the flow direction, producing a helical flow within the microchannel. In addition, as the flow transitions from a no-slip to shear-free interface, it accelerates in the *x* direction from rest to a velocity that can approach 50% of the average velocity in the channel. To conserve mass, fluid is swept downward toward the top of the air-water interface, producing a strong three-dimensional flow local to the superhydrophobic surface. The influence of this tertiary flow can be amplified by reducing the height of the microchannel (Ou et al. 2007). The authors compared their results to a hydrophilic grooved surface in the Wenzel state similar in design to the channels first proposed by Stroock et al. (2002a,b) and demonstrated that the presence of the shear-free interface produced a twofold increase in the rate of mixing.

Slip-Amplified Diffusion-Osmotic Flow

Above we focus only on pressure-driven flows; however, in the field of microfluidics, flows are often actuated through surface-driven transport techniques. In electro-osmotic flow (the most

popular of these techniques), a near-plug flow is generated within a microchannel by the flow of dissociated ions in an electric field applied along the length of the microchannel (Karniadakis et al. 2005). A small boundary layer exists near the wall with the velocity varying over the thickness of the Debye length, λ_D, which is typically on the order of nanometers but depends on the fluid and salt concentration. In pressure-driven flows, the slip length must be on the order of the channel height for any significant drag reduction to be achieved (see Equation 2). However, for electro-osmotic flow, the slip length needs only to be on the order of the Debye length, $b \approx \lambda_D$, to have a significant effect on the flow (Ajdari & Bocquet 2006, Joly et al. 2004). Thus, it is possible for slip on smooth hydrophobic surfaces to have a large impact on electro-osmotic flows even in channels much larger than the slip lengths (Huang et al. 2008). However, as Huang et al. (2008) recently showed, increasing the slip length further by using superhydrophobic surfaces does not produce any additional enhancement to the electro-osmotic flow. Although the air-water interface is shear free, its presence produces no additional driving force for the flow because it is charge neutral. The addition of the air-water interface essentially has no net impact on electro-osmotic flow. Diffusio-osmotic flow, conversely, is quite different.

Diffusio-osmotic flow is flow induced by solute concentration gradients. Unlike electro-osmotic flow, the ions driving the diffusion-osmotic flow can have direct interaction with the air-water interface through either charge repulsion or specific adsorption. Thus, the driving force does not vanish over the air-water interface. Huang et al. (2008) demonstrated through molecular dynamic simulations that the increase in flow rate resulting from slip along superhydrophobic surfaces scales as $(1 + b/\lambda_D)$ for diffusion-osmotic flows. Such an effect could conceivably increase flow rates by a factor of $b/\lambda_D \approx 10^2 - 10^4$ and holds great promise in microfluidic and nanofluidic applications.

SLIP ON SUPERHYDROPHOBIC SURFACES: TURBULENT FLOWS

Drag reduction in turbulent flows can be achieved through a number of different mechanisms, including the addition of polymers to the fluid (Virk 1975) and the addition of bubbles (Sanders et al. 2006) or air layers (Elbing et al. 2008, Fukuda et al. 2000), compliant walls (Hahn et al. 2002), and riblets (Walsh 1990). A number of recent studies have investigated the use of superhydrophobic surfaces as a new passive technique for reducing drag in turbulent flows. Geometrically, riblets appear similar to the superhydrophobic surfaces; however, their scale and function are completely different. Riblets are ridges in the Wenzel state that are aligned in the flow direction. They reduce drag in turbulent flows by disrupting the transverse motion of the fluid at the surface, thereby moving near-wall turbulent structures further from the wall (Walsh 1990). Riblets only perform well within a limited range of Reynolds numbers and can have derogatory effects outside of their designed range (Choi et al. 1991, Walsh 1990). To function, a spacing between riblets, $w^+ = w/\nu(\tau_w/\rho)^{1/2}$, between $10 < w^+ < 30$ wall units must be maintained (Goldstein & Tuan 1998), where ν is the viscosity, τ_w is the wall shear stress, and ρ is the density of the liquid. The superhydrophobic microfeatures used to produce turbulent drag reduction are typically too small to simultaneously produce a riblet effect.

Air-layer drag reduction is another turbulent drag-reduction technique similar to superhydrophobic surfaces. Here air is continuously injected into the boundary layer to produce an uninterrupted vapor layer existing between the solid surface and the water. Thus the goal is to generate the continuous-flow analog of a Leidenfrost drop. Elbing et al. (2008) demonstrated that air layers can produce nearly complete elimination of skin-friction drag. The authors demonstrated the existence of three distinct regions: bubble drag reduction at low air-injection rates at which drag reductions up to 20% can be achieved, a transitional region at moderate injection rates, and

a continuous air layer at large air-injection rates. In an interesting study, Reed (1994) utilized millimeter-sized ridges to capture and stabilize the injected air and form a continuous air layer between the ridges. Reed (1994) noted that hydrophobic walls, with features much too large to produce a superhydrophobic effect, exhibited an enhanced ability to form air layers.

Fundamentally, the superhydrophobic drag-reduction mechanism—an effective area reduction of the solid-liquid boundary—should be independent of whether the flow is laminar or turbulent. In turbulent flows, a thin laminar sublayer exists very near to the wall, to a height, y, in wall units of $y^+ = y/\nu(\tau_w/\rho)^{1/2} = 5$ (Pope 2003). Fukagata et al.'s (2006) theoretical analysis suggested the way in which a small alteration of the laminar sublayer can affect the entire turbulent boundary layer and subsequently alter the drag. This effect is demonstrated in the direct numerical simulation studies of Min & Kim (2004) who performed turbulent channel flow simulations at a friction Reynolds number of $Re_\tau = (\tau_w/\rho)^{1/2}H/\nu = 180$ with an arbitrary, but not unreasonable, slip length boundary imposed both parallel and perpendicular to the flow direction. Their simulations demonstrated a decrease in wall shear stress with increasing slip length applied parallel to the flow direction, but an increase in wall shear stress for slip applied perpendicular to the flow direction.

More recently, Martell et al. (2009a,b) used direct numerical simulation to study the turbulent channel flows over superhydrophobic surfaces containing periodic arrays of micropost and microridge geometries. The top surface of each microfeature was taken to be no slip, whereas the suspended liquid-gas interface between the microfeatures was simulated as flat and shear-free. Only one side of the microchannel was modeled as superhydrophobic, with the other side having a no-slip boundary condition. A series of velocity and Reynolds stress profiles is shown in **Figure 7** for channel flow at a friction Reynolds number of $Re_\tau = 180$ over a superhydrophobic surface containing a series of microridges in the flow direction. The velocity profiles in **Figure 7*a*** show a slip velocity and drag reduction that increase with both the increasing microfeature spacing, w, and surface coverage of the shear-free air-water interface, $(1 - \phi_S)$. As seen in **Figure 7*b***, the peak values of the Reynolds stress, R_{11}, decreased near and shifted toward the superhydrophobic surface, resulting in an asymmetric Reynolds stress profile. As expected, with the reduced shear

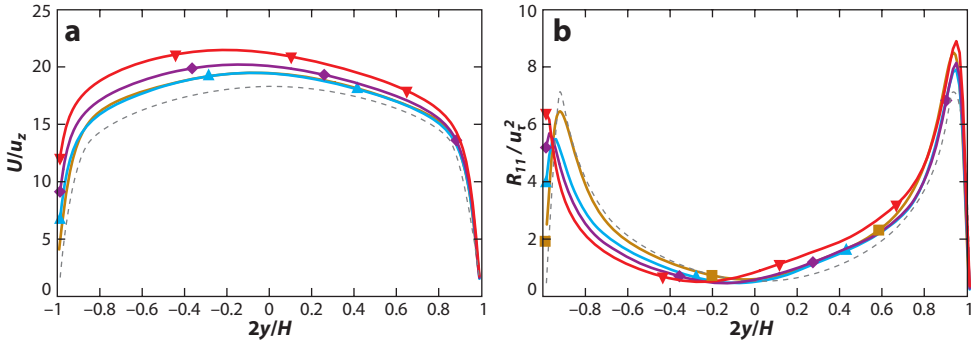

Figure 7

(*a*) Velocity profiles and (*b*) Reynolds stress profiles predicted from direct numerical simulation of channel flow at a friction Reynolds number of $Re_\tau = 180$ over superhydrophobic surfaces with 15 μm wide ridges spaced 15 μm apart (*gold squares*), 30 μm wide ridges spaced 30 μm apart (*blue triangles*), 30 μm wide ridges spaced 50 μm apart (*purple diamonds*), and 30 μm wide ridges spaced 90 μm apart (*red triangles*). Additionally, smooth channel flow is shown for reference (*dotted gray lines*). The symbols differentiate lines and do not reflect actual data points. Figure taken from Martell, Perot, Rothstein, Direct numerical simulations of turbulent flows over superhydrophobic surfaces, *J. Fluid Mech.*, 620:31–41, 2009 © Cambridge Journals, published by Cambridge University Press, reproduced with permission.

stress on the superhydrophobic surface, the turbulence levels decreased. These effects increased with increasing slip velocity and were consistent for all the microridge and micropost geometries simulated. In their most recent simulations, Martell et al. (2009a,b) showed that unlike in laminar flows, in turbulent flows, increasing the flow rate and Reynolds number results in an increase in the superhydrophobic drag reduction.

There are only a few experimental studies of superhydrophobic drag reduction in the turbulent regime (Balasubramanian et al. 2004, Daniello et al. 2009, Gogte et al. 2005, Henoch et al. 2006, Watanabe et al. 1999). Gogte et al. (2005) observed drag reduction in turbulent flow over a hydrofoil coated with an unstructured superhydrophobic surface consisting of hydrophobically modified sandpaper. Drag reductions of up to 18%, based on combined skin friction and form drag, were reported for the hydrofoil. The overall drag reduction on the hydrofoil decreased with increasing Reynolds number. However, only the total drag was reported, and the individual contribution of friction and form drag was not deconvoluted. Balasubramanian et al. (2004) observed similar results for flow over an ellipsoidal model coated with an unstructured superhydrophobic surface.

Daniello et al. (2009) used a rectangular flow cell with smooth and superhydrophobic PDMS walls with 30 μm and 60 μm wide microridges spaced 30 μm and 60 μm apart, respectively. They performed pressure-drop measurements, as well as PIV measurements, to investigate the drag-reducing ability of superhydrophobic surfaces in turbulent flows at Reynolds numbers between $2000 < Re = HU/\nu < 10{,}000$, where U is the mean fluid velocity. Their experiments were designed to probe both the laminar and turbulent flow regimes; transition to turbulence occurs at approximately $Re > 3000$ (Pope 2003). **Figure 8** shows an example of the velocity profiles measured for a series of microridges $d = 30$ μm wide and spaced $w = 30$ μm apart. The effect of the superhydrophobic wall is not observed for the low–Reynolds number experiments. This is consistent with preview data points in the laminar or transitional regime (Ou et al. 2004, Ou & Rothstein 2005). In laminar flows, superhydrophobic surfaces of similar size and geometry demonstrated slip lengths that were independent of flow rate and approximately $b \approx 25$ μm

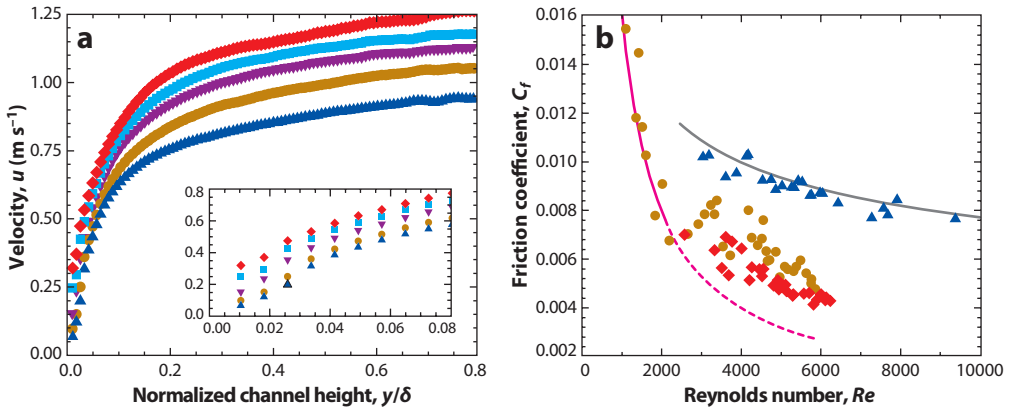

Figure 8

Velocity profiles and friction coefficient measurements for channel flow past superhydrophobic surfaces. (*a*) The Reynolds number increases from $Re = 5300$ (*dark blue triangles*) to $Re = 8000$ (*red diamonds*) over 30 μm wide ridges spaced 30 μm apart. (*b*) Reduced friction coefficients are noted for channel flow over superhydrophobic surfaces, with 30 μm wide ridges spaced 30 μm apart (*gold circles*) and 60 μm wide ridges spaced 60 μm apart (*red diamonds*). Smooth surface data (*dark blue triangles*) and predicted smooth values (*lines*) are shown for comparison. Figure adapted from Daniello R, Waterhouse NE, Rothstein JP. 2009. Turbulent drag reduction using superhydrophobic surfaces. *Phys. Fluids* 2009 © American Institute of Physics, reproduced with permission.

(Ou & Rothstein 2005). For the channels studied in these experiments, Equation 2 predicts a drag reduction of approximately 1%. Additionally, for small slip lengths, one can approximate the expected slip velocity by $u_{slip} = 8Ub/H$, which is also on the order of a couple percent of the average free stream velocity and is at or below the resolution of their PIV measurements.

As the Reynolds number is increased and the flow becomes fully turbulent, Daniello et al.'s (2009) PIV measurements (**Figure 8**) show a substantial slip velocity along the superhydrophobic wall. As the inset of **Figure 8** clearly shows, the magnitude of the slip velocity increases with increasing Reynolds number. Substantial reductions in friction coefficient were noted for both microridge geometries in the turbulent regime (**Figure 8*b***). The maximum drag reduction from pressure-drop measurements approached $D_R = (\tau_{no-slip} - \tau_{SH})/\tau_{no-slip} \approx 50\%$, whereas slip lengths of nearly $b \approx 80\,\mu m$ were observed at the largest Reynolds numbers tested. Similar trends were observed for the 60 μm wide ridges spaced 60 μm apart (**Figure 8*b***), at which the drag reduction became measurable at even smaller Reynolds numbers and slip lengths of over $b > 100\,\mu m$ were achieved.

Daniello et al. (2009) hypothesize that we can understand the physical origins of the critical Reynolds number for the onset of drag reduction by analyzing the relevant length scales in the flow. If the drag reduction and the slip length were dependent on the microridge geometry and channel dimensions alone (as is the case in laminar flows), then one would expect to find the drag reduction and slip length to be independent of the Reynolds number, which it clearly is not. In turbulent flows, however, there is a third length scale of importance: the thickness of the viscous sublayer that extends out to $y^+ = 5$. Although the viscous sublayer thickness does not change in wall units, it decreases in dimensional form with increasing Reynolds number, $y_{vsl} = 5H/Re_\tau$. Close to the wall (where viscous stresses dominate), Philip's (1972a,b) analytical solutions show that the influence of the shear-free air-water interface on the velocity profile extends into the flow at a distance roughly equal to the microridge spacing, w. Thus for the superhydrophobic surface to impact the turbulent flow, the microridge spacing must approach the thickness of the viscous sublayer, $w \approx y_{vsl}$. This is consistent with Daniello et al.'s (2009) PIV results. As the thickness of the viscous sublayer is reduced further, the impact of the superhydrophobic surface increases. This analysis suggests that an asymptote in the turbulent drag reduction is likely in the limit of very large Reynolds numbers, at which the microridges are much larger than the viscous sublayer. In this limit, the drag reduction should approach a limit of $D_R = 1 - \phi_s$, as momentum is only transferred from the solid fraction of the superhydrophobic surface and the viscous sublayer is thin enough that the no-slip and shear-free portions of the surface can be considered independently. This is consistent with the asymptotic value of the pressure-drop measurements presented in **Figure 8*b***.

SUMMARY AND OUTLOOK

This review presents a detailed account of our current understanding of flow past superhydrophobic surfaces. It discusses a wealth of experimental, computational, and theoretical results that demonstrate how the combination of surface roughness and hydrophobicity can be used to engineer large slip at the liquid-solid interface by utilizing the shear-free liquid-vapor interface, which, under the right conditions, can be supported between the peaks of the surface roughness. Although the use of superhydrophobic surfaces for drag reduction is a relatively young research field, we hope this review convinces the reader that the drag-reducing properties of superhydrophobic surfaces in pressure-driven laminar flows are now fairly well understood. That is not to say that there are no challenges remaining; there are a number of important questions left to answer and quite a bit of work left to do if we are to utilize these surfaces to their full potential.

In laminar and turbulent flows, the question of surface optimization still remains. Although the performance trends are generally understood, only a small subset of possible surface geometries has been investigated. In droplet dynamics, the importance of a second topological length scale for the elimination of contact-angle hysteresis has been demonstrated (Gao & McCarthy 2006b). The impact, if any, of a second topological length scale on drag reduction in a continuous flow is still unknown. Additionally, superhydrophobic surfaces are inherently fragile. Large features cannot maintain an interface and slip under large static pressures, whereas smaller features may be too delicate to survive the large shear stresses that can occur, especially in turbulent flows. The development of surfaces capable of maintaining an interface and performance under large static pressures is still needed if the use of superhydrophobic surfaces is to become mainstream.

Using superhydrophobic surfaces to produce drag reduction in turbulent flows is still in its infancy, and as such there are a number of interesting fundamental questions to be examined. Recent experimental and computation work appears to indicate that drag reduction increases with increasing Reynolds number and a reduction of the thickness of the viscous sublayer, but a more detailed understanding of the physical nature of this scaling has yet to be presented. The upper limit of superhydrophobic drag reduction is still unknown in the turbulent regime. Daniello et al. (2009) hypothesize that the maximum drag reduction would approach the fraction of the shear-free interface along the superhydrophobic surface as the Reynolds number increased. However, it is also conceivable that at small solid fractions, the momentum transferred from the superhydrophobic surface may be insufficient to maintain a turbulent flow and the limiting case may be that of a superlaminar flow. Additionally, questions about the importance of free-surface curvature and compliance on turbulent drag reduction need to be investigated. Finally, the range of experiments and simulations needs to be extended to much larger Reynolds numbers and over a wide variety of different flow geometries.

A number of applications for superhydrophobic surfaces, such as their use for enhancing mixing in microfluidic devices (Ou et al. 2007), have already been developed. There is a multitude of other clever applications of superhydrophobic surfaces waiting to be developed. In a recent work, Maynes et al. (2008) used numerical simulations to investigate heat transfer from superhydrophobic surfaces. Although the reduced liquid-solid contact of the superhydrophobic surfaces resulted in a reduction in the heat transfer coefficient, the reduction in the drag coefficient was more significant. Thus, using superhydrophobic surfaces, they demonstrated that up to a 30% improvement in the heat transfer rate could be achieved for the same pumping power. These simulations have yet to be confirmed by experiments or extended into the turbulent flow regime, but this technology could prove quite useful for the liquid cooling of microelectronic devices. Thus the future of superhydrophobic surfaces holds considerable promise for a wide range of fluid dynamic and heat transfer applications.

DISCLOSURE STATEMENT

The author is not aware of any affiliations, memberships, funding, or financial holdings that might be perceived as affecting the objectivity of this review.

ACKNOWLEDGMENTS

The author would like to express his sincere thanks to both current and former undergraduate and graduate students whose work constituted a large part in this review article, specifically, J. Ou, G. Moss, N. Waterhouse, M. Martell, and R. Daniello. The author would also like to thank B. Perot for many years of collaboration in this area, J. Bico for sparking his interest in superhydrophobic

surfaces, and T. McCarthy for teaching him how to fabricate these surfaces. Finally, the author acknowledges a 3M Nontenured Faculty Award and the Office of Naval Research for the partial support provided under grant N00014-06-1-0497.

LITERATURE CITED

Ajdari A, Bocquet L. 2006. Giant amplification of interfacially driven transport by hydrodynamic slip: diffusio-osmosis and beyond. *Phys. Rev. Lett.* 96:186102

Balasubramanian AK, Miller AC, Rediniotis OK. 2004. Microstructured hydrophobic skin for hydrodynamic drag reduction. *AIAA J.* 42:411–14

Barrat J-L, Bocquet L. 1999. Large slip effect at a nonwetting fluid-solid interface. *Phys. Rev. Lett.* 82:4671–74

Barthlott W, Neinhuis C. 1997. Purity of the sacred lotus, or escape from contamination in biological surfaces. *Planta* 202:1–8

Bartolo D, Bouamrirene F, Verneuil E, Buguin A, Silberzan P, Mouline S. 2006. Bouncing or sticky droplets: impalement transitions on superhydrophobic micropatterned surfaces. *Europhys. Lett.* 74:299–305

Batchelor GK. 1985. *An Introduction to Fluid Dynamics*. Cambridge, UK: Cambridge Univ. Press

Baudry J, Charlaix E, Tonck A, Mazuyer D. 2001. Experimental evidence for a large slip effect at a nonwetting fluid-surface interface. *Langmuir* 17:5232–36

Bhushan B, Jung YC. 2006. Micro- and nanoscale characterization of hydrophobic and hydrophilic leaf surfaces. *Nanotechnology* 17:2758–72

Bico J, Marzolin C, Quéré D. 1999. Pearl drops. *Europhys. Lett.* 47:220–26

Bico J, Thiele U, Quéré D. 2002. Wetting of textured surfaces. *Colloids Surf. A* 206:41–46

Blake TD. 1990. Slip between a liquid and a solid: D.M. Tolstoi's (1952) theory reconsidered. *Colloids Surf. A* 47:134–45

Bocquet L, Tabeling P, Manneville S. 2006. Comment on "Large slip of aqueous liquid flow over a nanoengineered superhydrophobic surface". *Phys. Rev. Lett.* 97:109601

Bouzigues CI, Bocquet L, Charlaix E, Cottin-Bizonne C, Cross B, et al. 2008. Using surface force apparatus, diffusion and velocimetry to measure slip lengths. *Philos. Trans. R. Soc. A* 366:1455–68

Bush JWM, Hu DL, Prakash M. 2008. The integument of water-walking arthropods: form and function. *Adv. Insect Physiol.* 34:117–92

Cassie ABD, Baxter S. 1944. Wettability of porous surfaces. *Trans. Faraday Soc.* 40:546–51

Chen W, Fadeev AY, Hsieh MC, Oner D, Youngblood JP, McCarthy TJ. 1999. Ultrahydrophobic and ultralyophobic surfaces: some comments and examples. *Langmuir* 15:3395–99

Choi C-H, Johan K, Westin A, Breuer KS. 2003. Apparent slip flows in hydrophilic and hydrophobic microchannels. *Phys. Fluids* 15:2897–902

Choi C-H, Kim CJ. 2006. Large slip of aqueous liquid flow over a nanoengineered superhydrophobic surface. *Phys. Rev. Lett.* 96:066001

Choi C-H, Ulmanella U, Kim J, Ho C-M, Kim C-J. 2006. Effective slip and friction reduction in nanograted superhydrophobic microchannels. *Phys. Fluids* 18:087105

Choi H, Moin P, Kim J. 1991. On the effect of riblets in fully developed laminar channel flows. *Phys. Fluids A* 3:1892–96

Cottin-Bizonne C, Barentin C, Charlaix E, Bocquet L, Barrat J-L. 2004. Dynamics of simple liquids at heterogeneous surfaces: molecular dynamics simulations and hydrodynamic description. *Eur. Phys. J. E* 15:427–38

Cottin-Bizonne C, Barrat J-L, Bocquet L, Charlaix E. 2003. Low-friction flows of liquid at nanopatterned interfaces. *Nat. Mater.* 2:237–40

Cottin-Bizonne C, Cross B, Steinberger A, Charlaix E. 2005. Boundary slip on smooth hydrophobic surfaces: intrinsic effects and possible artifacts. *Phys. Rev. Lett.* 94:056102

Daniello R, Waterhouse NE, Rothstein JP. 2009. Turbulent drag reduction using superhydrophobic surfaces. *Phys. Fluids* 21:085103

de Gennes PG, Brochard-Wyart F, Quéré D. 2004. *Capillarity and Wetting Phenomena: Drops, Bubbles, Pearls, Waves*. New York: Springer. 291 pp.

Denn MM. 2001. Extrusion instabilities and wall slip. *Annu. Rev. Fluid Mech.* 33:265–87
Dussan EB. 1979. On the spreading of liquids on solid surfaces: static and dynamic contact lines. *Annu. Rev. Fluid Mech.* 11:371–400
Elbing BR, Winkel ES, Lay KS, Ceccio SL, Dowling DR, Perlin M. 2008. Bubble-induced skin-friction drag reduction and the abrupt transition to air-layer drag reduction. *J. Fluid Mech.* 612:201–36
Fang G, Li W, Wang X, Qiao G. 2008. Droplet motion on designed microtextured superhydrophobic surfaces with tunable wettability. *Langmuir* 24:11651–60
Freund JB. 2003. The atomic detail of a wetting/dewetting flow. *Phys. Fluids* 15:L33–36
Fukagata K, Kasagi N, Koumoutsakos P. 2006. A theoretical prediction of friction drag reduction in turbulent flow by superhydrophobic surfaces. *Phys. Fluids* 18:051703
Fukuda K, Tokunaga J, Nobunaga T, Nakatani T, Iwasaki T, Kunitake Y. 2000. Frictional drag reduction with air lubricant over a superwater-repellent surface. *J. Marine Sci. Technol.* 5:123–30
Gao L, McCarthy TJ. 2006a. Contact angle hysteresis explained. *Langmuir* 22:6234–37
Gao L, McCarthy TJ. 2006b. The "lotus effect" explained: two reasons why two length scales of topography are important. *Langmuir* 22:2966–67
Gao L, McCarthy TJ. 2006c. A perfectly hydrophobic surface (θ(A)/θ(R) = 180°/180°). *J. Am. Chem. Soc.* 128:9052–53
Gao X, Jiang L. 2004. Water-repellent legs of water striders. *Nature* 432:36
Gogte S, Vorobieff P, Truesdell R, Mammoli A, van Swol F, et al. 2005. Effective slip on textured superhydrophobic surfaces. *Phys. Fluids* 17:051701
Goldstein DB, Tuan T-C. 1998. Secondary flow induced by riblets. *J. Fluid Mech.* 363:115–51
Goldstein S, ed. 1965. *Modern Developments in Fluid Dynamics: An Account of Theory and Experiment Relating to Boundary Layers, Turbulent Motion and Wakes*. New York: Dover. 702 pp.
Hahn S, Je J, Choi H. 2002. Direct numerical simulation of turbulent channel flow with permeable walls. *J. Fluid Mech.* 450:259–85
Harting J, Kunert C, Herrmann HJ. 2006. Lattice Boltzmann simulations of apparent slip in hydrophobic microchannels. *Europhys. Lett.* 75:328–34
Henoch C, Krupenkin TN, Kolodner P, Taylor JA, Hodes MS, et al. 2006. Turbulent drag reduction using superhydrophobic surfaces. *Collect. Tech. Pap. 3rd AIAA Flow Control Conf.* 2:840–44
Hocking LM. 1976. A moving fluid interface on a rough surface. *J. Fluid Mech.* 76:801–17
Huang DM, Cottin-Bizonne C, Ybert C, Bocquet L. 2008. Massive amplification of surface-induced transport at superhydrophobic surfaces. *Phys. Rev. Lett.* 101:064503
Hyvaluoma J, Harting J. 2008. Slip flow over structured surfaces with entrapped microbubbles. *Phys. Rev. Lett.* 100:246001
Israelachvili JN. 1992. *Intermolecular and Surface Forces*. London: Academic. 450 pp.
Jin S, Huang P, Park J, Yoo JY, Breuer KS. 2004. Near-surface velocity using evanescent wave illumination. *Exp. Fluids* 37:825–33
Joly L, Ybert C, Bocquet L. 2006. Probing the nanohydrodynamics at liquid-solid interfaces using thermal motion. *Phys. Rev. Lett.* 96:046101
Joly L, Ybert C, Trizac E, Bocquet L. 2004. Hydrodynamics within the electric double layer on slipping surfaces. *Phys. Rev. Lett.* 93:257805
Joseph P, Cottin-Bizonne C, Benoit J-M, Ybert C, Journet C, et al. 2006. Slippage of water past superhydrophobic carbon nanotube forests in microchannels. *Phys. Rev. Lett.* 97:156104
Joseph P, Tabeling P. 2005. Direct measurement of the apparent slip length. *Phys. Rev. E* 71:035303
Karniadakis G, Beskok A, Aluru N. 2005. *Microfluids and Nanofluidics*. New York: Springer
Kim J, Kim C-J. 2002. *Nanostructured surfaces for dramatic reduction of flow resistance in droplet-based microfluidics*. Presented at IEEE Int. Conf. MEMS, Las Vegas
Lafuma A, Quéré D. 2003. Superhydrophobic states. *Nat. Mater.* 2:457–60
Lauga E, Brenner MP, Stone HA. 2007. Microfluidics: the no-slip boundary condition. In *Handbook of Experimental Fluid Dynamics*, ed. J Foss, C Tropea, AL Yarin, pp. 1219–40. New York: Springer
Lauga E, Stone HA. 2003. Effective slip in pressure driven Stokes flow. *J. Fluid Mech.* 489:55–77
Lee C, Choi C-H, Kim C-J. 2008. Structured surfaces for giant liquid slip. *Phys. Rev. Lett.* 101:064501

Mahadevan L, Pomeau Y. 1999. Rolling droplets. *Phys. Fluids* 11:2449–53
Martell MB, Perot JB, Rothstein JP. 2009a. Direct numerical simulations of turbulent flows over superhydrophobic surfaces. *J. Fluid Mech.* 620:31–41
Martell MB, Rothstein JP, Perot JB. 2009b. The effect of Reynolds number on turbulent flows over superhydrophobic surfaces. Submitted manuscript
Maxwell JC. 1879. On stresses in rarified gases arising from inequalities of temperature. *Philos. Trans. R. Soc. London* 170:231–56
Maynes D, Jeffs K, Woolford B, Webb BW. 2007. Laminar flow in a microchannel with hydrophobic surface patterned microribs oriented parallel to the flow direction. *Phys. Fluids* 19:093603
Maynes D, Webb BW, Davies J. 2008. Thermal transport in a microchannel exhibiting ultrahydrophobic microribs maintained at constant temperature. *J. Heat Transf.* 130:022402
Min T, Kim J. 2004. Effects of hydrophobic surface on skin-friction drag. *Phys. Fluids* 16:L55–58
Navier CLMH. 1823. Memoire sur les lois du mouvement des fluides. *Mem. Acad. R. Sci. Inst. France* 6:389–440
Oner D, McCarthy TJ. 2000. Ultrahydrophobic surfaces: effects of topography length scales on wettability. *Langmuir* 16:7777–82
Ou J. 2007. *Laminar flow control using ultrahydrophobic surfaces*. Ph.D. thesis. Univ. Mass., Amherst
Ou J, Moss GR, Rothstein JP. 2007. Enhanced mixing in laminar flows using ultrahydrophobic surfaces. *Phys. Rev. E* 76:016304
Ou J, Perot JB, Rothstein JP. 2004. Laminar drag reduction in microchannels using ultrahydrophobic surfaces. *Phys. Fluids* 16:4635–60
Ou J, Rothstein JP. 2005. Direct velocity measurements of the flow past drag-reducing ultrahydrophobic surfaces. *Phys. Fluids* 17:103606
Philip JR. 1972a. Flows satisfying mixed no-slip and no-shear conditions. *Z. Angew. Math. Phys.* 23:353–72
Philip JR. 1972b. Integral properties of flows satisfying mixed no-slip and no-shear conditions. *Z. Angew. Math. Phys.* 23:960–68
Pit R, Hervet H, Leger L. 1999. Friction and slip of a simple liquid at a solid surface. *Tribol. Lett.* 7:147–52
Pope SB. 2003. *Turbulent Flows*. Cambridge, UK: Cambridge Univ. Press
Quéré D. 2008. Wetting and roughness. *Annu. Rev. Mater. Res.* 38:71–99
Quéré D, Azzopardi M-J, Delattre L. 1998. Drops at rest on a tilted plane. *Langmuir* 14:2213–16
Reed JC. 1994. Using grooved surfaces to improve the efficiency of air injection drag reduction methods in hydrodynamic flows. *J. Ship Res.* 38:133–36
Reyssat M, Pepin A, Marty F, Chen Y, Quéré D. 2006. Bouncing transitions on microtextured materials. *Europhys. Lett.* 74:306–12
Reyssat M, Yeomans JM, Quéré D. 2008. Impalement of fakir drops. *Europhys. Lett.* 81:26006
Richard D, Quéré D. 2000. Bouncing water drops. *Europhys. Lett.* 50:769–75
Richardson S. 1973. On the no-slip boundary condition. *J. Fluid Mech.* 59:707–19
Sakai M, Song JH, Yoshida N, Suzuki S, Kameshima Y, Nakajima A. 2006. Direct observation of internal fluidity in a water droplet during sliding on hydrophobic surfaces. *Langmuir* 22:4906–9
Sanders WC, Winkel ES, Dowling DR, Perlin M, Ceccio SL. 2006. Bubble friction drag reduction in a high-Reynolds-number flat-plate turbulent boundary layer. *J. Fluid Mech.* 552:353–80
Sbragaglia M, Benzi R, Biferale L, Succi S, Toschi F. 2006. Surface roughness-hydrophobicity coupling in microchannel and nanochannel flows. *Phys. Rev. Lett.* 97:204503
Sbragaglia M, Prosperetti A. 2007. A note on the effective slip properties for microchannel flows with ultrahydrophobic surfaces. *Phys. Fluids* 19:043603
Schnell E. 1956. Slippage of water over nonwettable surfaces. *J. Appl. Phys.* 27:1149–52
Shastry A, Case MJ, Bohringer KF. 2006. Directing droplets using microstructured surfaces. *Langmuir* 22:6161–67
Steinberger A, Cottin-Bizonne C, Kleimann P, Charlaix E. 2007. High friction on a bubble mattress. *Nat. Mater.* 6:665–68
Stroock AD, Dertinger SK, Whitesides GM, Ajdari A. 2002a. Patterning flows using grooved surfaces. *Anal. Chem.* 74:5306–12
Stroock AD, Dertinger SKW, Ajdari A, Mezic I, Stone HA, Whitesides GM. 2002b. Chaotic mixer for microchannels. *Science* 295:647–51

Thompson PA, Troian SM. 1997. A general boundary condition for liquid flow at solid surfaces. *Nature* 389:360–62

Tolstoi DM. 1952. Molecular theory for slippage of liquids over solid surfaces. *Dokl. Akad. Nauk. SSSR* 85:1089–92 (In Russian)

Tretheway DC, Meinhart CD. 2002. Apparent fluid slip at hydrophobic microchannel walls. *Phys. Fluids* 14:L9–12

Truesdell R, Mammoli A, Vorobieff P, van Swol P, Brinker CJ. 2006. Drag reduction on a patterned superhydrophobic surface. *Phys. Rev. Lett.* 97:044504

Vinogradova OI. 1999. Slippage of water over hydrophobic surfaces. *Int. J. Miner. Process.* 56:31–60

Virk PS. 1975. Drag reduction fundamentals. *AIChE J.* 21:625–56

Voronov RS, Papavassiliou DV, Lee LL. 2008. Review of fluid slip over superhydrophobic surfaces and its dependence on the contact angle. *Ind. Eng. Chem. Res.* 47:2455–77

Watanabe K, Yanuar, Udagawa H. 1999. Drag reduction of Newtonian fluid in a circular pipe with highly water-repellent wall. *J. Fluid Mech.* 381:225–38

Walsh MJ. 1990. Riblets. In *Viscous Drag Reduction in Boundary Layers*, ed. DM Bushnell, JN Hefner, pp. 203–62. Reston, VA: Am. Inst. Aeronaut. Astronaut.

Wenzel RN. 1936. Resistance of solid surfaces to wetting by water. *Ind. Eng. Chem.* 28:988–94

Wier KA, McCarthy TJ. 2006. Condensation on ultrahydrophobic surfaces and its effect on droplet mobility: Ultrahydrophobic surfaces are not always water repellant. *Langmuir* 22:2433–36

Wolfram E, Faust R. 1978. Liquid drops on a tilting plate, contact angle hysteresis and the Young contact angle. In *Wetting, Spreading and Adhesion*, ed. JF Padday, pp. 213–22. New York: Academic

Yang J-T, Chen JC, Huang K-J, Yeh JA. 2006. Droplet manipulation on a hydrophobic textured surface with roughened patterns. *J. Microelectromech. Syst.* 15:697–707

Ybert C, Barentin C, Cottin-Bizonne C, Joseph P, Bocquet L. 2007. Achieving large slip with superhydrophobic surfaces: scaling laws for generic geometries. *Phys. Fluids* 19:123601

Young T. 1805. An essay on the cohesion of fluids. *Philos. Trans. R. Soc. London* 95:65–87

Zhu Y, Granick S. 2001. Rate-dependent slip of Newtonian liquids at smooth surfaces. *Phys. Rev. Lett.* 87:096105

Zhu Y, Granick S. 2002. Limits of hydrodynamic no-slip boundary conditions. *Phys. Rev. Lett.* 88:106102

Annual Review of
Fluid Mechanics

Volume 42, 2010

Contents

Indexes

Errata

An online log of corrections to *Annual Review of Fluid Mechanics* articles may be found at http://fluid.annualreviews.org/errata.shtml